

Special Issue:

In honor of Prof. David Y.H. Pui for his "50 Years of Contribution in Aerosol Science and Technology" (III)

OPEN ACCESS 

Received: November 30, 2022

Revised: January 12, 2023

Accepted: February 6, 2023

*** Corresponding Author:**

romay001@umn.edu

Publisher:

Taiwan Association for Aerosol
Research

ISSN: 1680-8584 print

ISSN: 2071-1409 online

© Copyright: The Author(s).

This is an open access article distributed under the terms of the [Creative Commons Attribution License \(CC BY 4.0\)](https://creativecommons.org/licenses/by/4.0/), which permits unrestricted use, distribution, and reproduction in any medium, provided the original author and source are cited.

Design of Round-Nozzle Inertial Impactors Review with Updated Design Parameters

Francisco J. Romay^{1*}, Estíbaliz García-Ruiz²

¹Mechanical Engineering Department, College of Science & Engineering, University of Minnesota, Minneapolis, MN, USA

²Department of Chemical & Environmental Engineering, University of the Basque Country, UPV/EHU, Bilbao, Spain

ABSTRACT

Round-nozzle inertial impactors are widely used aerosol measuring instruments to characterize the mass and chemical composition of airborne aerosol particles as a function particle aerodynamic diameter. This article summarizes the most important design considerations with updated recommended design parameters taken from our review of published research articles and discusses some of the more common non-idealities seen in the operation and performance of inertial impactors. With this information, it is now possible to design a cascade impactor with near-ideal particle separation performance, and with stage cutpoints that can be predicted with excellent accuracy and verified experimentally using state-of-the-art calibration techniques.

Keywords: Inertial impactor, Cascade impactor, Impactor design parameters, Stokes number

1 INTRODUCTION

Inertial impactors continue to be used today for the collection of size segregated aerosol particles, for mass and chemical composition characterization as a function of particle aerodynamic diameter. The first impactors date back to the 1860s, and Marple (2004) provides a comprehensive review of the history of impactors from 1860s to the early 2000s. Impactors are used in many important applications such as indoor and outdoor air pollution (Cass *et al.*, 2000), industrial process aerosols (Kero *et al.*, 2015), pharmaceutical inhalers (Taki *et al.*, 2010), combustion aerosols from engines (Schauer *et al.*, 2008), forest fires (Costa *et al.*, 2022), nanoparticle characterization (Curwin and Bertke, 2011), biological aerosols (Appert *et al.*, 2012), and others. The beauty of inertial impactors is that users can easily understand how they work because they are simple devices that rely solely on the ability of airborne particles to deviate from fluid streamlines in the vicinity of an obstacle. This inertial separation principle led to the development of the single nozzle impactor, where particles are accelerated by a nozzle towards a flat plate (Fig. 1(a)). This basic geometry can result in a very sharp separation between particles that impact the plate, and particles that are able to go around the plate (Fig. 1(b)). Marple (1970) conducted the first fundamental study of inertial impactors by numerical flow field simulation and particle trajectory calculations to determine the collection efficiency curve of impactors, as a function of several parameters such as Stokes number, Reynolds number, jet-to-plate distance, and nozzle throat length (see Fig. 1). Rader and Marple (1985) updated the original numerical simulations (Marple and Liu, 1974) by adding ultra-Stokesian drag and particle interception to the collection efficiency predictions. This work has led to the proper design of several cascade impactors (Chen *et al.*, 2018; Chien *et al.*, 2015; Marjamäki *et al.*, 2000; Marple *et al.*, 2003a, 1995, 1991) by selecting design parameters that resulted in experimentally calibrated collection efficiency curves that are usually in excellent agreement with Marple's theoretical predictions. In the past 30 years, a lot of work has been done by researchers to better understand the performance of inertial impactors, particularly to include the effect of gravity on the collection of large particles, the



Fig. 1. (a) Single nozzle inertial impactor; (b) Ideal and actual collection efficiency curve as a function of Stokes number (i.e., \sqrt{Stk}).

effect of the cross-flow in the collection efficiency of multi-nozzle impactors, the particle bounce that occurs when sampling solid particles and how to avoid it, the unwanted deposition of particles on the back side of the nozzles, the formation of secondary particle deposits between nozzles, the formation of halo-type particle deposits away from the primary impactation zone, and other non-ideal behavior of impactors. A recent paper on inertial impactors (Le and Tsai, 2021) provides a comprehensive review of design and practical aspects such as particle bounce, re-entrainment, and overloading effects, as well as some of the typical applications.

This paper attempts to summarize and consolidate all these aspects that characterize the realistic performance of conventional inertial impactors with round nozzles, and provides a list of the main design parameters with its recommended ranges (Table 1), that will result in the near-ideal performance of a multi-jet cascade impactor with predictable collection efficiency curves that can be verified experimentally using conventional modern calibration techniques. We are excluding in this paper a discussion on virtual impactors, where the impactation plate is replaced by a minor flow tube, and a fraction of the flow is used to separate the particles by inertia.

2 MAIN DESIGN PARAMETERS

This paper will consider the design of multi-jet cascade impactors with round nozzles. While the analysis can be extended to impactors with rectangular nozzles, the great majority of commercially available impactors use circular nozzles, so we are purposely discussing impactors with round nozzles.

2.1 Stokes Number

The Stokes number is the main parameter that characterizes the performance of inertial impactors, defined as the ratio of the particle stopping distance calculated at the average nozzle exit velocity V_0 , to the nozzle radius $W/2$, where W is the nozzle diameter. For a single or multiple nozzle impactor the Stokes number is calculated as (Marple and Liu, 1974):

$$Stk = \frac{C(d_p) d_p^2 \rho_p V_0}{9 \mu W} \quad (1)$$

$$V_0 = \frac{4Q}{n\pi W^2} \quad (2)$$

where $C(d_p)$ is the slip correction factor, d_p is the particle diameter, ρ_p is the particle density, μ is



Table 1. Recommended impactor design parameters.

Impactor Design Parameter	Recommended Value	Comments
Stokes Number ($\sqrt{Stk_{50}}$)	0.489 for Re = 500 0.498 for Re = 1,500 0.507 for Re = 2,200	These values come from numerical simulations for laminar and turbulent flow models (García-Ruiz <i>et al.</i> , 2019b).
Reynolds Number (Re)	500 to 3,000	For stages with cutpoints below 100-nm Re can be as low as 200.
Jet-to-Plate Distance (S/W)	1 to 5 (for sharper collection efficiency curves). 5 to 10 (for nanometer stages where larger values of S are required).	For stages with cutpoints below 100-nm S/W can be as high as 15, preferably around 10 to maintain $\sqrt{Stk_{50}}$ close to 0.50.
Cross Flow Parameter ($Wn/4D_c$)	< 1.2	This parameter applies mainly to submicron impactor stages with multi-jet nozzles.
Nozzle Spacing Parameter (A/W)	≥ 4	This parameter applies mainly to super-micron impactor stages with mm sized nozzles.
Nozzle Geometry and Configuration	Conical tapered nozzles followed by straight throat. Hexagonal, Radial, Concentric Rings, or Random nozzle patterns.	For stages with cutpoints below 100-nm nozzles with a gradual contraction are preferred. For a small number of nozzles the pattern can be a single ring.
Gravitational Parameter (Fr)	$Fr > 500$ and $Re > 1,500$	Important for super-micron impactor stages; Values of $\sqrt{Stk_{50}}$ are lower when gravity plays a role.
Pressure Drop (ΔP)	Pressure drop should be optimized by increasing the number of nozzles while maintaining other design parameters within acceptable values.	The impactor pressure drop is dominated by the lower stages with submicron cutpoints. Avoid square cylindrical nozzles with lower discharge coefficients.

the absolute gas viscosity, Q is the total volumetric flow rate, and n is the number of nozzles. The square root of the Stokes number is typically considered as a dimensionless particle diameter. Considering a typical sigmoidal collection efficiency curve, as shown in Fig. 1(b), the diameter corresponding to the 50% collection efficiency is defined as the cutpoint of the impactor. Therefore,

$$d_{p,50} = \sqrt{\frac{9\mu W}{C(d_p)\rho_p V_0}} \sqrt{Stk_{50}} \quad (3)$$

where $d_{p,50}$ is the nominal cutpoint, and Stk_{50} is the Stokes number for which the collection efficiency is 50%. It is important to point out that $d_{p,50}$ is usually converted to the corresponding aerodynamic diameter based on particles with the density of water. In this case, Eq. (3) becomes

$$d_{a,50} = \sqrt{\frac{9\mu W}{C(d_a)\rho_0 V_0}} \sqrt{Stk_{50}} \quad (4)$$

where $d_{a,50}$ is the aerodynamic cutpoint diameter, and ρ_0 is the density of water (i.e., 1 g cm^{-3}). The slip correction factor in Eq. (4) is calculated for the aerodynamic diameter d_a .

Rader and Marple (1985) recommend using a $\sqrt{Stk_{50}}$ of 0.495 for the design of impactors assuming that the Reynolds number Re , and the dimensionless jet-to-plate diameter S/W are within the recommended ranges discussed later. A more recent numerical study (García-Ruiz *et al.*, 2019b) using modern CFD models with a much finer computational domain resulted in a small variation of $\sqrt{Stk_{50}}$ with the Reynolds number. These $\sqrt{Stk_{50}}$ values are 0.489, 0.508 and 0.518 for Reynolds of 500, 1500 and 3000 respectively and for laminar flow, while for a (Wilcox) k-w

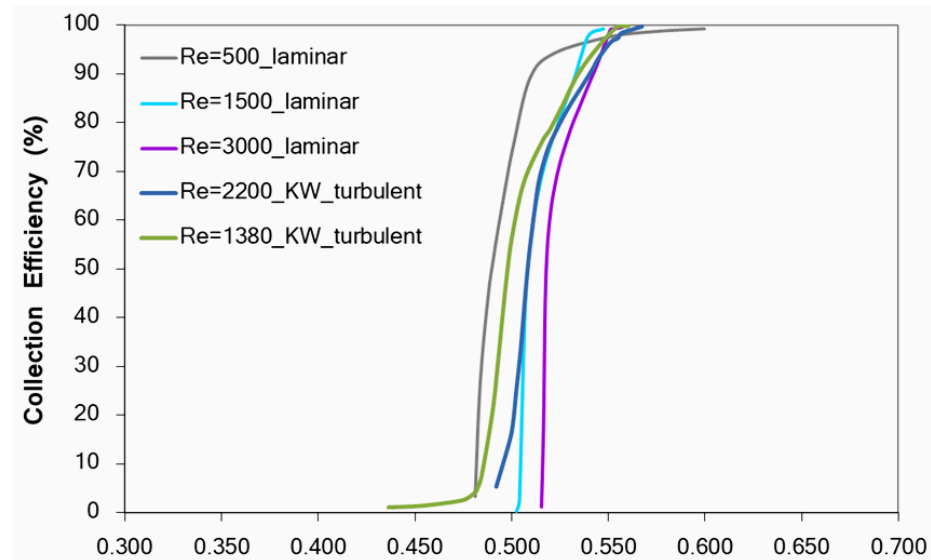
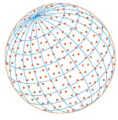


Fig. 2. Collection efficiency curves for a single nozzle impactor as a function of Reynolds number using laminar flow with a fine computational mesh, and turbulent flow (KW model) with a medium computational mesh (García-Ruiz *et al.*, 2019b).

turbulence flow model, the $\sqrt{Stk_{50}}$ are 0.498 and 0.507 for Reynolds 1380 and 2210 respectively (see Fig. 2). Therefore, we recommend using these more refined $\sqrt{Stk_{50}}$ values when designing new impactors.

2.2 Reynolds Number

The Reynolds number has an important effect on the performance of inertial impactors. The Reynolds number defines the flow regime in the region of particle separation. Reynolds number is defined as

$$Re = \frac{\rho_g V_0 W}{\mu} \quad (5)$$

where ρ_g is the gas density. The Reynolds number affects the shape of the collection curve and the values of $\sqrt{Stk_{50}}$, particularly for low and high values. However, Marple and Liu (1974) found that if the Reynolds number was between 500 and 3000, the effect of Reynolds number was minimum, and that the collection efficiency curves had sharp characteristics ideal for particle separation with a nearly constant value of $\sqrt{Stk_{50}}$. For smaller values of Reynolds number, the collection efficiency curves become shallower and shift to the right due to increased viscous effects. For larger Reynolds numbers, a more pronounced tail appears at larger particle sizes due to ultrastokesian drag, leading to a lower sharpness of cut (Rader and Marple, 1985). Therefore, to simplify the impactor design, particularly for cascade impactors with several multi-nozzle stages, it is recommended to maintain Reynolds numbers between 500 and 3000, so that the collection efficiency curves and corresponding cutpoints can be predicted from conventional impactor theory based on numerical simulation by CFD models. It is important to mention that when trying to extend the dynamic sizing range of cascade impactors, both for large (i.e., $> 10 \mu\text{m}$) and very small (i.e., $< 50 \text{ nm}$) particles, it is possible to see some impactor stages with Reynolds numbers slightly outside this recommended range (e.g., NanoMOUDI impactor, Marple and Olson, 1999). In these cases, it becomes imperative to determine the cutpoint of these stages experimentally, since deviations from theory can be expected. Therefore, it is recommended to stay within the range of Re between 500 and 3000, to avoid additional costly trial and error calibrations to determine the cutpoint and sharpness of cut. The Reynolds number also affects the formation of secondary deposits and particle losses on the backside of the nozzles, as well as the influence of gravity, but these effects will be discussed later in this paper.



2.3 Dimensionless Jet-to-Plate Distance (S/W)

The dimensionless jet-to-plate distance affects the impactor sharpness of cut, but the value of $\sqrt{Stk_{50}}$ is nearly independent of S/W , if it is maintained between 1 and 5 (Rader and Marple, 1985). A value of $S/W = 1$ results in the sharpest collection efficiency curve with a typical geometrical standard deviation or $GSD < 1.2$, where the GSD is typically calculated as (Marple and Olson, 2011):

$$GSD = \sqrt{\frac{d_{a,84}}{d_{a,16}}} \quad (6)$$

where $d_{a,84}$ and $d_{a,16}$ are the aerodynamic diameters for 84% and 16% collection efficiencies respectively. In practice, it is not always possible to maintain S/W values of 1, particularly as the nozzle diameters become very small for collecting finer particles. The minimum value of S that can be maintained in a precisely machined impactor is 0.5 to 1.0 mm, so as the nozzles reach sub-millimeter dimensions, larger jet-to-plate distances are required. For example, in the MOUDI impactor, the values of S/W vary from 1 for upper stages, to a value of 11 for the last 2 stages with cutpoints of 100 nm and 56 nm. Using S/W values larger than 1 result in lower sharpness of cut on the collection efficiency curves, as clearly seen in the published MOUDI efficiency curves for stages 6 to 10 (Marple *et al.*, 1991). Also, when using S/W values larger than 4, it is possible to see a change in the $\sqrt{Stk_{50}}$ values. Chien *et al.* (2015) reported a linear increase of $\sqrt{Stk_{50}}$ with S/W for stages 8, 9 and 10 of the NMCI impactor for S/W values between 4 and 20. Therefore, when designing impactor stages with nanometer cutpoints (< 100 -nm) that require small nozzles (i.e., < 0.10 -mm) and larger S/W values, experimental calibration is necessary to determine the stage cutpoints accurately.

The design parameters discussed so far, and their recommended ranges come from flow and particle trajectory simulations for a single nozzle impactor. However, they can also be used for designing multi-nozzle impactors as long these nozzles act independently of each other, which means that the acceleration jets do not interact with each other. This can be accomplished by ensuring that the nozzles are sufficiently separated to prevent jet-to-jet interactions. The following two parameters address this issue in the design of cascade impactors.

2.4 Cross-Flow Parameter

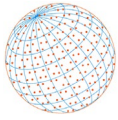
The cross-flow parameter (Fang *et al.*, 1991) is defined as:

$$CFP = \frac{Wn}{4D_c} < 1.2 \quad (7)$$

where n is the number of nozzles, and D_c is the cluster diameter (i.e., the diameter where all the nozzles are clustered). In the analysis by Fang *et al.* (1991), it was demonstrated experimentally that if the CFP was above 1.2, the cross flow exiting the stage interferes with some of the jets, leading to incomplete impaction, and collection curves not reaching 100% efficiency. But for $CFP < 1.2$, the collection efficiency curves are sigmoidal and reach 100% collection efficiency. The cross-flow parameter becomes critical when designing impactor stages with very low cutpoints smaller than 100-nm, requiring a large number of small nozzles needed to reduce the larger pressure drop associated with impacting very small particles. The design of the micro-orifice collector in the Next Generation Pharmaceutical Impactor (Marple *et al.*, 2003a) required to increase the nozzle cluster diameter to 75-mm, to accommodate a total of 4032 nozzles of 70- μ m diameter, and ensuring the CFP was below the maximum recommended value of 1.2.

2.5 Dimensionless Nozzle Spacing Parameter

The dimensionless nozzle spacing parameter (i.e., NSP) can be defined as the ratio of the nozzle-to-nozzle distance A (measured from center to center), divided by the nozzle diameter W :



$$NSP = \frac{A}{W} \geq 4 \quad (8)$$

This parameter assumes that all the nozzles are equally spaced, even though in many impactor designs this is not always the case. The importance of this parameter becomes obvious when designing impactor stages with large super-micron cutpoints (typically larger than 5- μm aerodynamic diameter), which require nozzles of several millimeters in diameter. In this case, it is tempting to cluster the nozzles too close to each other (to save space), which leads to the formation of secondary line deposits (García-Ruiz *et al.*, 2019a; Rocklage *et al.*, 2013) observed in many impactor designs. Until recently, the nozzle spacing between large millimeter-sized impactor nozzles has been treated rather informally. García-Ruiz *et al.* (2019a, 2019b) conducted a detailed numerical and experimental study using a single stage impactor with 3 nozzles equally spaced in an equilateral triangle, with A/W values ranging from 2.5 to 8, and Reynolds numbers between 465 and 2210. For the lowest nozzle spacing of 2.5 W , secondary line deposits and premature half-moon primary deposits were observed for particles smaller than the impactor cutpoint, leading to collection efficiency curves with a pronounced tail on the low end of the curve (Fig. 3), and with a lower value of \sqrt{Stk}_{50} . The use of a Shear Stress Transport turbulence model to predict the strong recirculation induced by the jet-jet interactions, provided excellent agreement with the experimental results (Fig. 3). Therefore, this study recommends to use a minimum nozzle spacing parameter (i.e., NSP) of at least 4 to minimize the effects of the jet-to-jet interactions. While at NSP = 4 it was possible to still see some line deposits, their contribution to the total deposited mass was very small (under 2%, García-Ruiz *et al.*, 2019a).

2.6 Nozzle Geometry and Configuration

The typical nozzle shape of most impactors has a tapered conical entrance followed by a straight throat section with a length T equal to the nozzle diameter W (see Fig. 1). This nozzle geometry gives sufficient time for the particles to accelerate to the fluid velocity exiting the nozzle (Marple and Willeke, 1976), and is typical for the majority of commercially available impactors with some exceptions (e.g., the Andersen-type impactor and the ELPI impactor have cylindrical nozzles). Tapered nozzle entrances also have a lower pressure drop due to their higher discharge coefficient (see Section 2.9 on pressure drop). Impactor stages for nanometer particles (typically < 100-nm) are difficult to make with a tapered conical nozzle, so in this case it is common to see an abrupt

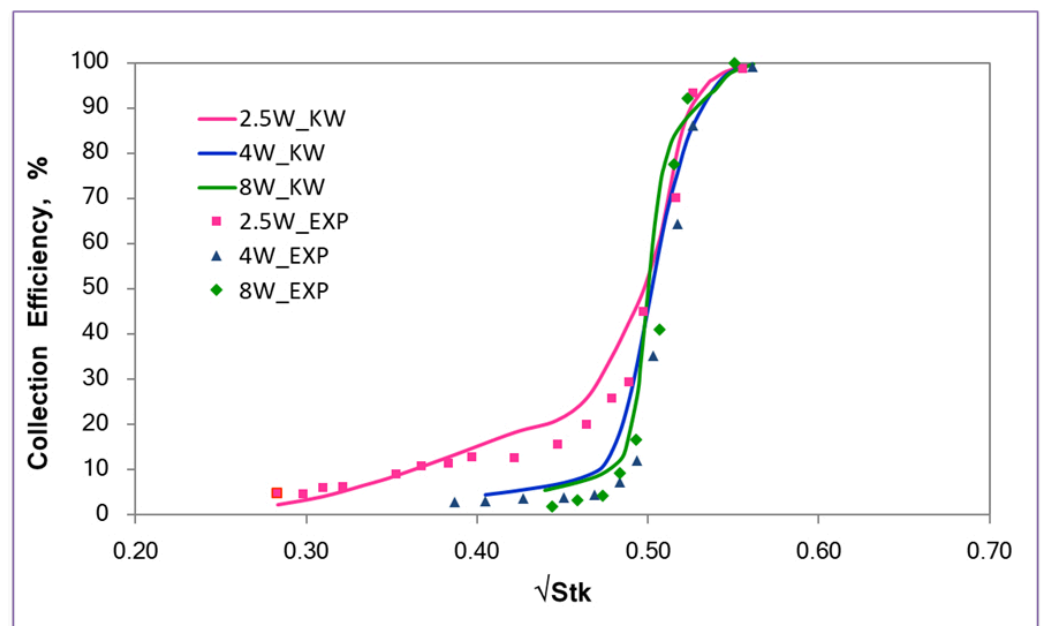
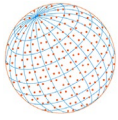


Fig. 3. Experimental and numerical collection efficiency curves at nozzle-to-nozzle spacings of 2.5 W , 6 W and 8 W for Reynolds of 2210 (data from García-Ruiz *et al.* (2019a, 2019b)).



contraction, such as in the stages 9 and 10 of MOUDI impactor. This can lead to faster nozzle clogging and associated particle losses as reported by Liu *et al.* (2013). By making the nozzles with a smooth transition, Liu *et al.* (2013) found that the lower stages of the NMCI cascade impactor were less prone to clogging when sampling high concentration combustion aerosols.

The nozzle configuration pattern in multi-nozzle impactors is normally left open to the designer, provided the nozzle spacing is adequate according to the discussion above. Kwon *et al.* (2002) conducted an experimental study using a 20-nozzle stage with 5 different nozzle configurations. The models had a conventional nozzle cluster design with either concentric rings or randomly spaced nozzles. The experimental values of $\sqrt{Stk_{50}}$ were in good agreement with theory, even though in some cases the nozzles were too close to each other, resulting in secondary line deposits and shallower efficiency curves. The nozzle configuration in stages 5 to 10 of the MOUDI impactor have nozzles in a randomly generated pattern. The NGI impactor (Marple *et al.*, 2003a, 2003b), has nozzles with different nozzle patterns (see Fig. 4) depending on the stage (a single ring for stage 2, a symmetric hexagonal pattern for stages 3, 4 and 5, and a radial pattern for stages 6 and 7). The values of $\sqrt{Stk_{50}}$ for stages 2 to 7 of the NGI stages fall within the range predicted by theory, an indication of a proper impactor design with collection efficiency curves that are reasonably sharp (GSD values of 1.11 to 1.21 at 30 L min⁻¹), and with minimum overlap between them.

2.7 Gravitational Parameter

Until now, we have not mentioned the effect of gravity in impactors. The reason is that gravity plays a role mainly for stages with large super-micron cutpoints (i.e., > 5 μm). The influence of gravity on the impactor performance can be inferred using the dimensionless Froude number defined as:

$$Fr = \frac{V_0^2}{gW} \quad (9)$$

Computational fluid dynamics models have been used to predict the effect of gravity as a function of Froude number and Reynolds number (Huang and Tsai, 2001; Rader and Marple, 1984). Gravity reduces the value of $\sqrt{Stk_{50}}$ and the steepness of the efficiency curves, particularly for values of $Fr < 500$ and $Re < 1,500$. However, experimental data from real impactors do not generally agree very well with these numerical models, so in cases where gravity plays a factor, experimental calibration is required to determine the cutpoint of the impactor. In most impactors that have a large cutpoint stage of about 10-μm, the efficiency curve is affected by gravity and

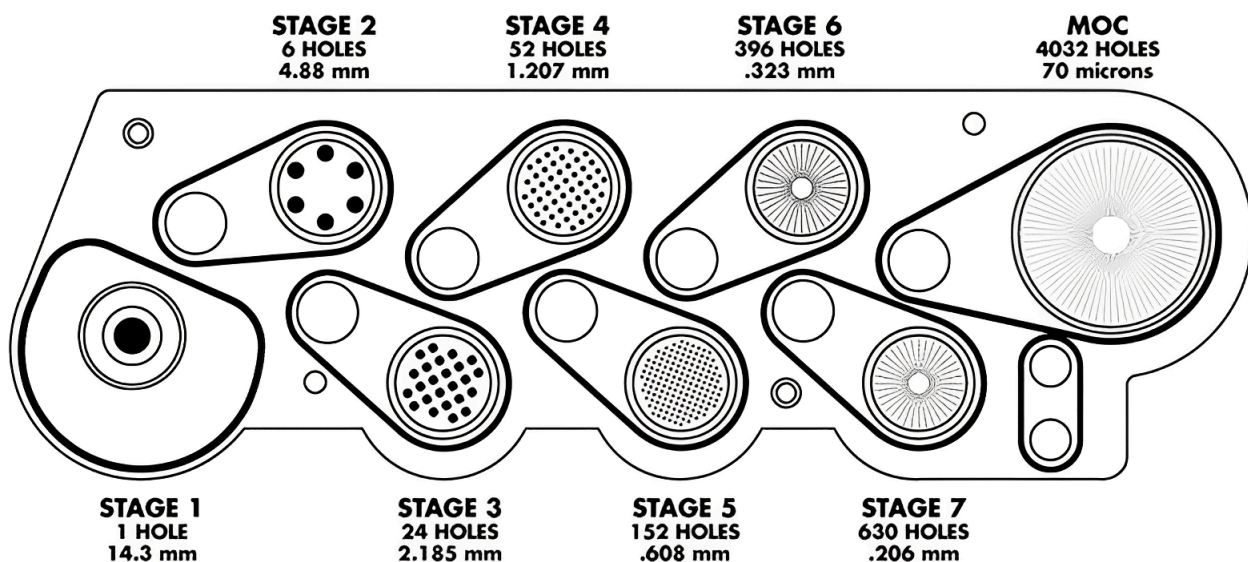
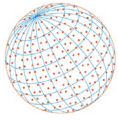


Fig. 4. Nozzle configuration of Next Generation Pharmaceutical Impactor (The Next Generation Pharmaceutical Impactor User Guide, Rev C, MSP Corporation, Shoreview, MN, 2008).



the value of $\sqrt{Stk_{50}}$ is below 0.50. For example, in the NGI impactor, stage 1 with a 11.7- μm cutpoint at 30 L min^{-1} has a $\sqrt{Stk_{50}}$ of 0.425 (Marple *et al.*, 2003b).

2.8 Particle Losses in Cascade Impactors

Proper design of a cascade impactor requires to minimize its internal particle losses, since particles that are lost on surfaces other than the impaction plates are typically not quantified, and therefore ignored in the mass size distribution determined from the impaction plate deposits. Particle losses depend on the type of particles being collected, being worse for liquid particles when compared to solid particles. A common type of particle losses is on the backside of the nozzle plates. These losses are dependent on the Reynolds number and on the nozzle spacing (García-Ruiz *et al.*, 2019a). They typically occur at higher Reynolds numbers and increase as the nozzle spacing decreases. For $S/W = 1$, García-Ruiz quantified these nozzle backside losses to be under 6% for liquid particles. In addition to the particle losses on the backside of the nozzles, particles can also be deposited on other surfaces, particularly on the inlet of the impactor where large particles can be lost by turbulent deposition in recirculation zones. For example, in the MOUDI impactor particles losses at the inlet can be as high as 35% and 20%, for liquid and solid particles respectively, and for particles larger than 10- μm in aerodynamic diameter (Marple *et al.*, 1991). Therefore, particular attention must be given to large particle losses near the inlet of impactors and in stages with ~ 10 μm cutpoints. One way to address the losses of large particles at the entrance of the impactor is to add a pre-separator with a large aerodynamic cutpoint. For the NGI impactor, a large particle pre-separator with two internal stages was designed for sampling dry powder inhaler formulations (Marple *et al.*, 2003a). This preseparator has a large enough volume and a special impaction well that can be filled with a solvent for the first coarse internal stage. This feature improves the performance of the impactor to remove particles larger than about 15- μm . The second internal stage has a conventional flat impaction plate with a sharper collection efficiency curve (Marple *et al.*, 2003b).

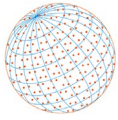
For particles between a few microns and 100-nm, interstage particle losses tend to be low in most impactors, if they are well designed. However, cascade impactors with stages for ultrafine particles below 100 nm can have significant losses by convection-diffusion (Durand *et al.*, 2014; Liu *et al.*, 2013). Liu *et al.* (2013) measured the particle losses by convection-diffusion in the MOUDI impactor, and found that for particles smaller than 40nm, particle losses can exceed 10%. These losses occur on all the internal surfaces of the impactor including the upper stages. To reduce particle losses by diffusion in a cascade impactor, the internal volume can be optimized to reduce the total residence time. Also, to collect nanoparticles by impaction low pressures are typically required, and this may enhance the evaporation of volatile and semivolatile particles. Geller *et al.* (2002) conducted tests to measure ammonium nitrite particle losses by volatilization in the 10-nm stage of the nanoMOUDI, and determined that they were negligible compared to the losses of the same ammonium nitrate particles collected in filters. This was explained by the reduced surface area and the formation of a stagnation flow boundary layer for the impactor deposits, resulting in lower losses of volatile particles collected in impactors as compared to filters. However, to reduce the extent of possible evaporation of collected semivolatile particles, it is recommended to optimize the pressure drop as explained in Section 2.9.

2.9 Impactor Pressure Drop

The total pressure drop of a cascade impactor is an important consideration during the design process, since the flow for the impactor is typically provided by a vacuum pump, whose capacity and minimum absolute pressure must be sufficient to draw the design inlet flow rate through the impactor. The pressure drop for a stage of a multi-nozzle impactor can be calculated as:

$$\Delta P = \frac{1}{2} \frac{\rho_g V_0^2}{C_d^2} = \frac{1}{2} \frac{\rho_g}{C_d^2} \left(\frac{4Q}{n\pi W^2} \right)^2 = \frac{8\rho_g Q^2}{n^2 \pi^2 C_d^2 W^4} \quad (10)$$

where C_d is the discharge coefficient of the nozzles, which is related to the shape of the nozzle, the formation of the “vena contracta”, and the frictional losses associated with the acceleration of the jet. The value of C_d is less than 1, and for typical tapered nozzles it varies between 0.7 and



0.9, while for a straight nozzle is 0.6. It is important to note that in the Eq. (10), the volumetric flow rate and density of the gas are at the actual pressure of the impactor stage. To reduce the magnitude of the pressure drop in the lower stages of a cascade impactor, the number of nozzles is increased as needed, while maintaining other parameters such as Reynolds number, cross-flow parameter, and jet-to-plate distance within recommended ranges. This optimization has resulted in the design of impactor stages with a cut-point as low as 10-nm, with nozzle diameters of about 50- μm , while operating at an absolute pressure of 10 kPa (Marple and Olson, 1999).

3 OTHER NON-IDEAL BEHAVIOR OF IMPACTORS

It is worth mentioning some other common observations on non-ideal behavior of impactors.

Several researchers have mentioned or studied the formation of halo particle deposits around the primary deposits (García-Ruiz *et al.*, 2019a; Rocklage *et al.*, 2013; Štefancová *et al.*, 2011). García-Ruiz *et al.* (2019a) explained that the halo is formed due to the boundary layer separation from the impaction plate, occurring while the air flow runs radially towards the outlet. That way, the particles with sufficient inertia, which are not able to follow the separation of the boundary layer, are inertially separated and deposited by gravity (Fig. 5).

Therefore, the analysis of the formation of the halo must consider both inertial and gravitational effects and the balance between them. The net effect of the halo on the collection efficiency curve is to reduce its slope and displace it towards smaller values of $\sqrt{Stk_{50}}$. That effect is increased by decreasing the Reynolds number and the Froude number. García-Ruiz *et al.* (2019a) concluded that halos are minimized for Reynolds numbers greater than 1000 and Froude numbers of about 10^4 . If these requirements cannot be met, the halo can be avoided with impaction plates small enough that prevent flow detachment. Therefore, the diameter of the impaction plate should be slightly larger than the nozzle cluster, ensuring that particles from all the jets can be collected on the impaction plate.

Particle bounce is one of the most common occurrences when using impactors, where particles that impact the collection surface bounce off, resulting in collection of these particles in the lower stages of the impactor, and skewing the mass size distribution towards smaller sizes.

Particle bounce in impactors can be effectively controlled by the application of anti-bounce coatings such as high-viscosity silicone oil to the impaction plates (Pak *et al.*, 1992), and this is



Fig. 5. Halo formation on impaction plate for 3-nozzle impactor at $A/W = 6$ and $Re = 1380$ (García-Ruiz *et al.*, 2019a).



the most common way to control impactor bounce. The application of such coatings is not always a desirable option, particularly when determining the composition of the collected particles, and there is a risk of interference in the chemical analysis of the collected particles (Fujitani *et al.*, 2006). Another way to reduce particle bounce is by conditioning the relative humidity of the sampled aerosol to near 70–80% RH (Vasilou *et al.*, 1999), where it was found that RH conditioned ambient aerosols were correctly sampled in the impactor with minimal particle bounce. This particle bounce reduction is attributed to the increased adhesion by capillary force between the adsorbed water on the particle and the impaction plate (Bateman *et al.*, 2014). Chen *et al.* (2016) devised a humidity conditioning system using Nafion[®] tubes to maintain the RH of the sampled aerosol to 65% RH on the QCM (quartz crystal microbalance) MOUDI impactor. Finally, the surface properties of impaction plates can also be modified by increasing its surface roughness or porosity (Huang *et al.*, 2001; Le *et al.*, 2019; Marjamäki and Keskinen, 2004), to reduce bounce and resuspension of particles after being collected. While these surface modification methods can be highly effective, the collection efficiency curves for these modified impaction substrates may deviate significantly from the theory presented in this paper, due to increased particle deposition by filtration mechanisms on the low end of the curve. Therefore, experimental calibrations are necessary to determine the performance of the impactor when porous impaction plates or filters are used for eliminating particle bounce.

Even when using sticky antibounce coatings to reduce particle bounce, excessive particle loading on impaction plates can result in particle deposits being blown-off from the substrates, and increasing the mass collected at lower stages or at the final filter. Tsai *et al.* (2012) designed a nanoparticle sampler using a 100-nm impactor micro-orifice stage, with a silicone-oil coated Teflon filter with internal rotation as the impaction substrate, eliminating particle bounce and extending the total collected nanoparticle mass capacity. Le *et al.* (2022) recently developed a novel single-stage nanoparticle impactor with a wetted impaction substrate designed to eliminate the effect of particle loading on the impactor performance. While it is possible to reduce particle bounce and re-entrainment by these specialized impactor designs, the easiest way to reduce the incidence of particle blow-off in cascade impactors, even when using anti-bounce coatings, is to limit the sampling time according to the expected mass concentration of the sampled aerosol, so that the total mass collected per stage is maintained within reasonable limits, to meet the requirements of the quantitative mass/composition analysis, and following guidelines provided by the impactor manufacturer.

4 CONCLUSIONS

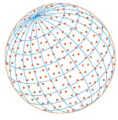
Inertial impactors with circular nozzles are basic aerosol instruments that can be designed using fundamental physical principles and specific design parameters that have been refined by many researchers during the last 50 years since the first study by Marple (1970) at the University of Minnesota. The five main parameters that define an inertial impactor with a sharp collection efficiency of a known aerodynamic diameter cutpoint are: (1) *Stokes number*, (2) *Reynolds number*, (3) *Dimensionless Jet-to-Plate distance*, (4) *Cross-flow parameter*, and (5) *Dimensionless Nozzle Spacing parameter*. By properly selecting appropriate values for these five parameters, several multi-stage cascade impactors have been designed and commercialized worldwide, and these impactors continue to be used for a wide range of applications encompassing the fields of air pollution, indoor air quality, combustion and industrial aerosols, pharmaceutical inhalers, bio-aerosols (bacteria, viruses and fungi), nanotechnology, and others. Like most aerosol instruments, inertial impactors also exhibit non-ideal behavior effects during practical use, such as particle bounce and re-entrainment of collected particles. These have also been studied and practical solutions exist to avoid performance issues that can lead to erroneous results. This paper includes results and recommendations from the most recent studies that enhance the understanding of inertial impactors, and summarizes how to best approach new impactor designs.

REFERENCES

Appert, J., Raynor, P.C., Abin, M., Chander, Y., Guarino, H., Goyal, S.M., Zuo, Z., Ge, S., Kuehn, T.H.



- (2012). Influence of suspending liquid, impactor type, and substrate on size-selective sampling of MS2 and adenovirus aerosols. *Aerosol Sci. Technol.* 46, 249–257. <https://doi.org/10.1080/02786826.2011.619224>
- Bateman, A.P., Belassein, H., Martin, S.T. (2014). Impactor apparatus for the study of particle rebound: Relative humidity and capillary forces. *Aerosol Sci. Technol.* 48, 42–52. <https://doi.org/10.1080/02786826.2013.853866>
- Cass, G.R., Hughes, L.A., Bhave, P., Kleeman, M.J., Allen, J.O., Salmon, L.G. (2000). The chemical composition of atmospheric ultrafine particles. *Philos. Trans. R. Soc. London, Ser. A* 358, 2581–2592. <https://doi.org/10.1098/rsta.2000.0670>
- Chen, M., Romay, F.J., Li, L., Naqwi, A., Marple, V.A. (2016). A novel quartz crystal cascade impactor for real-time aerosol mass distribution measurement. *Aerosol Sci. Technol.* 50, 971–983. <https://doi.org/10.1080/02786826.2016.1213790>
- Chen, M., Romay, F.J., Marple, V.A. (2018). Design and evaluation of a low flow personal cascade impactor. *Aerosol Sci. Technol.* 52, 192–197. <https://doi.org/10.1080/02786826.2017.1388498>
- Chien, C.L., Tien, C.Y., Liu, C.N., Ye, H., Huang, W., Tsai, C.J. (2015). Design and testing of the NCTU micro-orifice cascade impactor (NMCI) for the measurement of nanoparticle size distributions. *Aerosol Sci. Technol.* 49, 1009–1018. <https://doi.org/10.1080/02786826.2015.1089976>
- Costa, M.A.M., Amaral, S.S., Soares Neto, T.G., Cardoso, A.A., Santos, J.C., Souza, M.L., Carvalho, J.A. (2022). Forest fires in the Brazilian Amazon and their effects on particulate matter concentration, size distribution, and chemical composition. *Combust. Sci. Technol.* <https://doi.org/10.1080/00102202.2021.2019229>
- Curwin, B., Bertke, S. (2011). Exposure characterization of metal oxide nanoparticles in the workplace. *J. Occup. Environ. Hyg.* 8, 580–587. <https://doi.org/10.1080/15459624.2011.613348>
- Durand, T., Bau, S., Morele, Y., Matera, V., Bémer, D., Rousset, D. (2014). Quantification of low pressure impactor wall deposits during zinc nanoparticle sampling. *Aerosol Air Qual. Res.* 14, 1812–1821. <https://doi.org/10.4209/aaqr.2013.10.0304>
- Fang, C., Marple, V., Rubow, K. (1991). Influence of cross-flow on particle collection characteristics of multi-nozzle impactors. *J. Aerosol Sci.* 22, 403–415. [https://doi.org/10.1016/0021-8502\(91\)90001-X](https://doi.org/10.1016/0021-8502(91)90001-X)
- Fujitani, Y., Hasegawa, S., Fushimi, A., Kondo, Y., Tanabe, K., Kobayashi, S., Kobayashi, T. (2006). Collection characteristics of low-pressure impactors with various impaction substrate materials. *Atmos. Environ.* 40, 3221–3229. <https://doi.org/10.1016/j.atmosenv.2006.02.001>
- García-Ruiz, E., Romay, F.J., García, J.A., Cambra, J.F., Alonso, L., Legarreta, J.A. (2019a). Effect of nozzle spacing in the formation of primary and secondary deposits in multi-nozzle inertial impactors part I: Experimental study. *J. Aerosol Sci.* 136, 61–81. <https://doi.org/10.1016/j.jaerosci.2019.06.008>
- García-Ruiz, E., Romay, F.J., García, J.A., Iza, J.M., Cambra, J.F., Gangoiti, G., Legarreta, J.A. (2019b). Effect of nozzle spacing in the formation of primary and secondary deposits in multi-nozzle inertial impactors part II: Numerical study. *J. Aerosol Sci.* 136, 106–127. <https://doi.org/10.1016/j.jaerosci.2019.06.009>
- Geller, M.D., Kim, S., Misra, C., Sioutas, C., Olson, B.A., Marple, V.A. (2002). A methodology for measuring size-dependent chemical composition of ultrafine particles. *Aerosol Sci. Technol.* 36, 748–762. <https://doi.org/10.1080/02786820290038447>
- Huang, C.H., Tsai, C.J. (2001). Effect of gravity on particle collection efficiency of inertial impactors. *J. Aerosol Sci.* 32, 375–387. [https://doi.org/10.1016/S0021-8502\(00\)00086-0](https://doi.org/10.1016/S0021-8502(00)00086-0)
- Huang, C.H., Tsai, C.J., Shih, T.S. (2001). Particle collection efficiency of an inertial impactor with porous metal substrates. *J. Aerosol Sci.* 32, 1035–1044. [https://doi.org/10.1016/S0021-8502\(01\)00038-6](https://doi.org/10.1016/S0021-8502(01)00038-6)
- Kero, I., Naess, M.K., Tranell, G. (2015). Particle size distributions of particulate emissions from the ferroalloy industry evaluated by electrical low pressure impactor (ELPI). *J. Occup. Environ. Hyg.* 12, 37–44. <https://doi.org/10.1080/15459624.2014.935783>
- Kwon, S.B., Kim, M.C., Lee, K.W. (2002). Effects of jet configuration on the performance of multi-nozzle impactors. *J. Aerosol Sci.* 33, 859–869. [https://doi.org/10.1016/S0021-8502\(02\)00040-X](https://doi.org/10.1016/S0021-8502(02)00040-X)
- Le, T.C., Shukla, K.K., Sung, J.C., Li, Z., Yeh, H., Huang, W., Tsai, C.J. (2019). Sampling efficiency of low-volume PM₁₀ inlets with different impaction substrates. *Aerosol Sci. Technol.* 53, 295–308. <https://doi.org/10.1080/02786826.2018.1559919>



- Le, T.C., Tsai, C.J. (2021). Inertial impaction technique for the classification of particulate matters and nanoparticles: A review. *KONA Powder Part. J.* 38, 42–63. <https://doi.org/10.14356/kona.2021004>
- Le, T.C., Lin, C.H., Gong, W.C., Ždímal, V., Pui, D.Y.H., Tsai, C.J. (2022). Novel inertial impactor for nanoparticle classification without particle loading effect. *J. Aerosol Sci.* 159, 105879. <https://doi.org/10.1016/j.jaerosci.2021.105879>
- Liu, C.N., Awasthi, A., Hung, Y.H., Tsai, C.J. (2013). Collection efficiency and interstage loss of nanoparticles in micro-orifice-based cascade impactors. *Atmos. Environ.* 69, 325–333. <https://doi.org/10.1016/j.atmosenv.2012.12.003>
- Marjamäki, M., Keskinen, J., Chen, D.R., Pui, D.Y.H. (2000). Performance evaluation of the electrical low-pressure impactor (ELPI). *J. Aerosol Sci.* 31, 249–261. [https://doi.org/10.1016/S0021-8502\(99\)00052-X](https://doi.org/10.1016/S0021-8502(99)00052-X)
- Marjamäki, M., Keskinen, J. (2004). Effect of impaction plate roughness and porosity on collection efficiency. *J. Aerosol Sci.* 35, 301–308. <https://doi.org/10.1016/j.jaerosci.2003.09.001>
- Marple, V.A. (1970). A fundamental study of inertial impactors. Ph. D. Thesis, University of Minnesota, Minneapolis.
- Marple, V.A., Liu, B.Y.H. (1974). Characteristics of laminar jet impactors. *Environ. Sci. Technol.* 8, 648–654. <https://doi.org/10.1021/es60092a003>
- Marple, V.A., Willeke, K. (1976). Impactor design. *Atmos. Environ.* 10, 891–896. [https://doi.org/10.1016/0004-6981\(76\)90144-X](https://doi.org/10.1016/0004-6981(76)90144-X)
- Marple, V.A., Rubow, K.L., Behm, S.M. (1991). A microorifice uniform deposit impactor (MOUDI): Description, calibration, and use. *Aerosol Sci. Technol.* 14, 434–446. <https://doi.org/10.1080/02786829108959504>
- Marple, V.A., Olson, B.A., Miller, N.C. (1995). A low-loss cascade impactor with stage collection cups: Calibration and pharmaceutical inhaler applications. *Aerosol Sci. Technol.* 22, 124–134. <https://doi.org/10.1080/02786829408959732>
- Marple, V.A., Olson, B.A. (1999). A Micro-Orifice Impactor with Cut Sizes Down to 10 Nanometers for Diesel Exhaust Sampling. Generic Center for Respirable Dust, Pennsylvania State University, University Park, PA.
- Marple, V.A., Roberts, D.L., Romay, F.J., Miller, N.C., Truman, K.G., Van Oort, M., Olsson, B., Holroyd, M.J., Mitchell, J.P., Hochrainer, D. (2003a). Next generation pharmaceutical impactor (a new impactor for pharmaceutical inhaler testing). Part I: Design. *J. Aerosol Med.* 16, 283–299. <https://doi.org/10.1089/089426803769017659>
- Marple, V.A., Olson, B.A., Santhanakrishnan, K., Mitchell, J.P., Murray, S.C., Hudson-Curtis, B.L. (2003b). Next generation pharmaceutical impactor (a new impactor for pharmaceutical inhaler testing). Part II: Archival calibration. *J. Aerosol Med.* 16, 301–324. <https://doi.org/10.1089/089426803769017668>
- Marple, V.A. (2004). History of impactors—The first 110 years. *Aerosol Sci. Technol.* 38, 247–292. <https://doi.org/10.1080/02786820490424347>
- Marple, V.A., Olson, B.A. (2011). Sampling and Measurement Using Inertial, Gravitational, Centrifugal, and Thermal Techniques, in: Kulkarni, P., Baron, P.A., Willeke, K. (Eds.), *Aerosol Measurement*, John Wiley & Sons, Inc., Hoboken, NJ, USA, pp. 129–151. <https://doi.org/10.1002/9781118001684.ch8>
- Pak, S.S., Liu, B.Y.H., Rubow, K.L. (1992). Effect of coating thickness on particle bounce in inertial impactors. *Aerosol Sci. Technol.* 16, 141–150. <https://doi.org/10.1080/02786829208959544>
- Rader, D.J., Marple, V.A. (1884). Effect of particle gravitational forces on the calculation of impactor efficiency curves, in: *Aerosols: Science, Technology and Industrial Applications of Airborne Particles*, Elsevier, New York, pp. 123–126.
- Rader, D.J., Marple, V.A. (1985). Effect of ultra-stokesian drag and particle interception on impaction characteristics. *Aerosol Sci. Technol.* 4, 141–156. <https://doi.org/10.1080/02786828508959044>
- Rocklage, J.M., Marple, V.A., Olson, B.A. (2013). Study of secondary deposits in multiple round nozzle impactors. *Aerosol Sci. Technol.* 47, 1144–1151. <https://doi.org/10.1080/02786826.2013.823641>
- Schauer, J.J., Christensen, C.G., Kittelson, D.B., Johnson, J.P., Watts, W.F. (2008). Impact of ambient temperatures and driving conditions on the chemical composition of particulate



- matter emissions from non-smoking gasoline-powered motor vehicles. *Aerosol Sci. Technol.* 42, 210–223. <https://doi.org/10.1080/02786820801958742>
- Štefancová, L., Schwarz, J., Mäkelä, T., Hillamo, R., Smolík, J. (2011). Comprehensive characterization of original 10-stage and 7-stage modified bernier type impactors. *Aerosol Sci. Technol.* 45, 88–100. <https://doi.org/10.1080/02786826.2010.524266>
- Taki, M., Marriott, C., Zeng, X.M., Martin, G.P. (2010). Aerodynamic deposition of combination dry powder inhaler formulations in vitro: A comparison of three impactors. *Int. J. Pharm.* 388, 40–51. <https://doi.org/10.1016/j.ijpharm.2009.12.031>
- Tsai, C.J., Liu, C.N., Hung, S.M., Chen, S.C., Uang, S.N., Cheng, Y.S., Zhou, Y. (2012). Novel active personal nanoparticle sampler for the exposure assessment of nanoparticles in workplaces. *Environ. Sci. Technol.* 46, 4546–4552. <https://doi.org/10.1021/es204580f>
- Vasiliou, J.G., Sorensen, D., McMurry, P.H. (1999). Sampling at controlled relative humidity with a cascade impactor. *Atmos. Environ.* 33, 1049–1056. [https://doi.org/10.1016/S1352-2310\(98\)00323-9](https://doi.org/10.1016/S1352-2310(98)00323-9)